

# NASA Technical Paper 1548

LOAN COPY: RETURN TO  
AFWL TECHNICAL LIBRARY  
KIRTLAND AFB, N. M.



## The Wave Structures of the Eady Model of Baroclinic Instability

Jae Min Hyun and William W. Fowles

OCTOBER 1979





NASA Technical Paper 1548

# The Wave Structures of the Eady Model of Baroclinic Instability

Jae Min Hyun and William W. Fowles  
*George C. Marshall Space Flight Center  
Marshall Space Flight Center, Alabama*

**NASA**

National Aeronautics  
and Space Administration

**Scientific and Technical  
Information Branch**

1979



# TABLE OF CONTENTS

	Page
INTRODUCTION .....	1
FORMULATION AND EADY'S SOLUTION .....	2
RESULTS AND DISCUSSION .....	9
REFERENCES .....	21

# LIST OF ILLUSTRATIONS

Figure	Title	Page
1.	Propagation speed $C_R$ versus scaled wavenumber $K$ . . . . .	9
2.	Growth rate $KC_I$ versus scaled wavenumber $K$ . . . . .	10
3.	Amplitude and phase variations of the most unstable mode ( $K = 1.6061$ , $C_R = 0.5$ , $C_I = 0.1929$ ) . . . . .	11
4.	The $x$ - $z$ plot showing the interrelationships among the dynamical variables . . . . .	12
5.	Amplitude and phase variations of an unstable wave ( $K = 2.2$ , $C_R = 0.5$ , $C_I = 0.0961$ ) . . . . .	14
6.	Amplitude and phase variations of an unstable wave ( $K = 2.35$ , $C_R = 0.5$ , $C_I = 0.0476$ ) . . . . .	15
7.	Amplitude and phase variations of a marginally stable most ( $K = 2.3996$ , $C_R = 0.5$ , $C_I = 0.0$ ) . . . . .	17
8.	Amplitude and phase variations of a fast-propagating stable mode ( $K = 3.5$ , $C_R = 0.7131$ , $C_I = 0.0$ ) . . . . .	18
9.	Amplitude and phase variations of a slow-propagating stable mode ( $K = 3.5$ , $C_R = 0.2869$ , $C_I = 0.0$ ) . . . . .	19

# THE WAVE STRUCTURES OF THE EADY MODEL OF BAROCLINIC INSTABILITY

## INTRODUCTION

A number of baroclinic fluid models have been proposed to investigate the large-scale (synoptic scale) processes in geophysical fluid dynamical systems [1,2]. It is now generally understood that the initial development of the large-scale travelling waves in the westerlies in temperate latitudes may be modelled by use of a linear stability analysis of a structured zonal current of a baroclinic fluid. The fundamental source of energy for the growing disturbances is recognized to be the latitudinally differential solar heating, which creates a temperature gradient in the north-south direction.

Under the assumptions of geostrophic balance and hydrostatic approximation, which are appropriate for scales of long waves in the middle latitudes, systematic derivation of the scaled governing hydrodynamic equations of motion yields a set of approximate forms of equations known as the quasi-geostrophic equations [3].

Among several models, the well-known model of Eady [2], using the Boussinesq fluid approximation and neglecting the  $\beta$ -effect, allows ready analytical solutions; it captures the essential features of the baroclinic waves. In Eady's model, a (vertically) stably stratified zonal current is contained between two rigid, parallel, rotating, horizontal boundaries. Two principal results of the Eady model are that there is a short wavelength cutoff for the unstable wave region and that the short wavelength cutoff and the most unstable wavelength do not depend on the vertical wind shear.

In this report, the solutions of the Eady eigenvalue equation are recast into a somewhat more manageable form, and the propagation speed and the growth rate of baroclinic waves of varying sizes pertinent to the Eady model are computed. Another purpose of this report is to provide a comprehensive picture of the detailed wave structures, characterized by the amplitude and the phase variations of the relevant physical variables. This information has been available only piecemeal in the literature. Physical interpretations of the interrelationships among the detailed wave structures are given, which reveal important aspects of the mechanisms responsible for the energy transfer from the basic state to the growing waves.

This report complements Eady's original work, adding detailed information concerning the quasi-geostrophic baroclinic wave structures.

## FORMULATION AND EADY'S SOLUTION

The derivation of the quasi-geostrophic set of equations has been amply documented [3] and will not be repeated here. We shall recapitulate only the highlights of the basic assumptions embedded in the quasi-geostrophic set of equations.

Let the cartesian coordinate axes  $x, y, z$  refer to eastward, northward, and vertically upward directions, respectively, while  $u, v, w$  are the corresponding velocity components. A parallel flow in the  $x$ -direction of a vertically stably stratified Boussinesq fluid is confined within two horizontal rigid boundaries at  $z = 0$  and  $z = H$ . The vertical stratification of the fluid is described by (the horizontally averaged) Brunt-Väisälä frequency  $N(z)$ . We choose  $U$  to be a characteristic horizontal velocity,  $L$  a horizontal length scale,  $L/U$  the time scale, and  $f/2$  the rotation rate parallel to the  $z$ -axis.

The geostrophic balance is achieved when the Rossby number  $R_0$  is small, i.e.,

$$R_0 = U/(fL) \ll 1 \quad . \quad (1)$$

The comparable importance of stratification and rotation in the dynamical processes is expressed by the condition that the Froude number  $F(z)$  is of order unity, i.e.,

$$F(z) = (f^2 L^2)/(N^2 H^2) \sim 0(1) \quad . \quad (2)$$

The hydrostatic approximation is also necessary to the derivation of the quasi-geostrophic equations. Note that by invoking the hydrostatic approximation we do not allow the vertical acceleration term  $dw/dt$  in the vertical momentum equation; however, it is to be realized that the vertical velocity  $w$  itself is carried on in the formulation. Typically, the vertical velocity  $w$  is quite small, of the order of  $\delta R_0 U$ , where  $\delta = H/L$ , but because of vortex-tube

stretching the vertical velocity plays a principal role in the quasi-geostrophic formulations.

Systematic scaling of the equations of motion indicates that the pressure deviation from the horizontally averaged hydrostatic pressure, nondimensionalized by  $\rho_0 UfL$  where  $\rho_0$  is an average density for the Boussinesq fluid, is a nondimensional streamfunction  $\psi$  for the horizontal velocities. Then the nondimensional velocity components ( $u, v, w$ ) are

$$\begin{aligned} u &= -\psi_y \\ v &= \psi_x \\ w &= -F \left( \frac{\partial}{\partial t} - \psi_y \frac{\partial}{\partial x} + \psi_x \frac{\partial}{\partial y} \right) \psi_z \end{aligned} \quad (3)$$

in which ( $u, v$ ) are scaled by  $U$ ,  $w$  by  $\delta R_0 U$ , ( $x, y$ ) by  $L$ ,  $z$  by  $H$ , and  $t$  by  $L/U$ .

Under the above assumptions, we can write a single equation which expresses the conservation of potential vorticity

$$\left( \frac{\partial}{\partial t} - \psi_y \frac{\partial}{\partial x} + \psi_x \frac{\partial}{\partial y} \right) \left[ \psi_{xx} + \psi_{yy} + (F\psi_z)_z \right] = 0 \quad . \quad (4)$$

Now, let  $\psi = \psi_0(y, z)$  be a zonally uniform, time-independent solution of Eq. (4), associated with a zonal current  $u = -\psi_0 y$ . This solution is perturbed by  $\psi'$ , and normal-mode solutions are assumed for the disturbances, i. e.,

$$\psi' = R_e \{ \hat{\phi}(y, z) \exp[ik(x - Ct)] \} \quad . \quad (5)$$

and

$$|\psi'| \ll |\psi_0| \quad .$$

Consequently, the eigenvalue problem posed for the quasi-geostrophic normal-mode perturbation pressure can be written as

$$(u - C) [\hat{\phi}_{yy} + (F\hat{\phi}_z)_z - k^2 \hat{\phi}] + [\beta - u_{yy} - (Fu_z)_z] \hat{\phi} = 0 \quad (6)$$

with two rigid-lid boundary conditions

$$(u - C) \hat{\phi}_z - u_z \hat{\phi} = 0 \quad \text{on} \quad z = 0, 1 \quad . \quad (7)$$

In Eq. (6) the dimensionless zonal wavenumber  $k$  is considered real, and the eigenvalue  $C [\equiv C_R + i C_I]$  and the eigenfunction  $\hat{\phi}$  are generally complex, while  $\beta = d(R_0^{-1})/dy \cong \text{const.}$  represents the south-north variation of  $f$ .

The Eady model specializes to the case in which  $u = z$ ,  $\beta = 0$ ,  $F(z) = \text{const.}$ ; Thus Eqs. (6) and (7) reduce to

$$(z - C) [\hat{\phi}_{yy} + F\hat{\phi}_{zz} - k^2 \hat{\phi}] = 0 \quad . \quad (8)$$

and

$$(z - C) \hat{\phi}_z - \hat{\phi} = 0 \quad . \quad (9)$$

Separating out the  $y$  dependence as  $\hat{\phi} = \Phi(z) e^{i\ell y}$ , where  $\ell$  is required to be real, Eady obtained the closed form solutions:

$$\Phi(z) = A \exp(-Kz) - \left( \frac{1 - K C}{1 + K C} \right) \exp(Kz) \quad , \quad (10)$$

where

$$K = F^{-1/2} (k^2 + \ell^2)^{1/2} \quad (11)$$

and the eigenvalue  $C$  is given as

$$C = \frac{1}{2} \pm \frac{1}{2K} \left[ \left( \frac{K}{2} - \coth \frac{K}{2} \right) \left( \frac{K}{2} - \tanh \frac{K}{2} \right) \right]^{1/2} \quad , \quad (12)$$

where  $A$  is an arbitrary constant.

Equation (12) shows that there is a critical wavelength below which all waves are neutral ( $C_I = 0$ ). The critical neutral wavenumber  $K_C$  is computed to be

$$K_C = F^{-1/2} (k^2 + \ell^2)^{1/2} = 2.3994 \quad . \quad (13)$$

The most unstable wave, which is associated with the maximum growth rate  $k C_I$ , occurs when

$$F^{-1/2} (k^2 + \ell^2)^{1/2} = 1.6062 \quad . \quad (14)$$

The growth rate  $k C_I$  is maximized when  $\ell = 0$ , i. e., when the disturbances are of infinite extent in the south-north direction.

Note that in Eady's model, the zonal wavenumber  $k$  and the latitudinal wavenumber  $\ell$  always appear simultaneously in the combined form  $(k^2 + \ell^2)$ . As a consequence, apart from the fact that  $\ell = 0$  corresponds to the most rapidly growing mode, setting  $\ell = 0$  from the outset does not cause any loss of generality in the dynamics in Eady's model. However, it is worth pointing out

here that in attempting any improvement of Eady's solution by incorporating terms of higher order in  $R_0$ , neglecting the  $y$ -variation of solutions would give rise to inconsistency and erroneous interpretations [4].

Employing the following shorthand notations

$$Q_1 = 1 - K C_R ,$$

$$Q_2 = K C_I ,$$

$$Q_3 = 1 + K C_R ,$$

$$G_1(z) = (Q_2^2 + Q_3^2) \exp(-Kz) - (Q_1 Q_3 - Q_2^2) \exp(Kz) ,$$

$$G_2(z) = 2 Q_2 \exp(Kz) , \quad (15)$$

$\Phi(z)$  may be rewritten as

$$\Phi(z) = \left( \frac{A}{Q_2^2 + Q_3^2} \right) |(G_1^2 + G_2^2)^{1/2}| \exp [i \tan^{-1} (G_2/G_1)] . \quad (16)$$

Once the analytical expression for the pressure perturbation  $\Phi(z)$  is found, other dynamical variables may be derived from the quasi-geostrophic set. In view of the relation linking the latitudinal velocity component,

$$v = R_e \{ V(z) \exp[ik(x - Ct)] \} ,$$

to the pressure perturbation, we can write

$$V(z) = ik\Phi(z) ;$$

thus

$$V(z) = \left( \frac{A}{Q_2^2 + Q_3^2} \right) \left| (G_1^2 + G_2^2)^{1/2} \right| \times k \exp \left\{ i \left[ \tan^{-1} (G_2/G_1) + \frac{\pi}{2} \right] \right\}. \quad (17)$$

The vertical component of the relative vorticity,

$$\zeta = \text{Re} \{ Z(z) \exp[ik(x - Ct)] \},$$

may be derived from  $\zeta = \nabla^2 \psi$ ; thus

$$Z(z) = \left( \frac{A}{Q_2^2 + Q_3^2} \right) \left| (G_1^2 + G_2^2)^{1/2} \right| \times k^2 \exp \left\{ i \left[ \tan^{-1} (G_2/G_1) + \frac{\pi}{2} \right] \right\}. \quad (18)$$

Based on the thermodynamic relation in the quasi-geostrophic set, the dimensionless temperature perturbation,

$$\theta = \text{Re} \{ \Theta(z) \exp[ik(x - Ct)] \},$$

is given as  $\partial \psi' / \partial z$ . Hence,  $\Theta$  is expressed as

$$\Theta(z) = \left( \frac{A}{Q_2^2 + Q_3^2} \right) \left| (G_1'^2 + G_2'^2)^{1/2} \right| \exp[i \tan^{-1} (G_2'/G_1')] \quad , \quad (19)$$

where

$$G_1' = \frac{dG_1}{dz} \quad , \quad G_2' = \frac{dG_2}{dz} \quad .$$

Note that under the Boussinesq fluid assumption the nondimensional density perturbation  $\rho$  is simply given as  $\rho = -\theta$ .

We now proceed to find an expression for the vertical velocity,

$$w = \text{Re} \{ W(z) \exp[i k(x - Ct)] \} \quad .$$

From the quasi-geostrophic relations, we can show that

$$F^{-1} W = -i k(z - C) \Theta + V \quad . \quad (20)$$

By use of equations (17) and (19), and rearranging, we have

$$W(z) = \left( \frac{A}{Q_2^2 + Q_3^2} \right) \left| (J_1^2 + J_2^2)^{1/2} \right| \times k F \exp[i \tan^{-1}(-J_1/J_2)] \quad , \quad (21)$$

where

$$J_1 = (z - C_R) G_1' + C_I G_2' - G_1 \quad ,$$

$$J_2 = (z - C_R) G_2' - C_I G_1' - G_2 \quad .$$

Finally, we consider the horizontal divergence,

$$\text{div } V_H = \text{Re} \{ D(z) \exp[i k(x - Ct)] \} \quad .$$

After some algebraic manipulation, we can show that

$$D(z) = \left( \frac{A}{Q_2^2 + Q_3^2} \right) \left| (M_1^2 + M_2^2)^{1/2} \right| \times k^3 \exp[i \tan^{-1}(-M_1/M_2)] \quad . \quad (22)$$

where

$$M_1 = (z - C_R) G_1 + C_I G_2 \quad ,$$

$$M_2 = (z - C_R) G_2 - C_I G_1 \quad .$$

In summary, based on the pressure perturbation  $\Phi$  in equation (10), we have found expressions for the relevant dynamical variables in the Eady model. The variables are the latitudinal velocity component  $v$ , the vertical component of the relative vorticity  $\zeta$ , the temperature perturbation  $\theta$ , the vertical velocity  $w$ , and the horizontal divergence  $\text{div } V_H$  in equations (15) through (22).

## RESULTS AND DISCUSSION

Firstly, the eigenvalue  $C(= C_R + i C_I)$  of the Eady problem is computed. Figure 1 shows the propagation speed  $C_R$  as a function of the scaled horizontal wavenumber  $K$ . As was stated earlier,  $l = 0$ , which is the most rapidly growing mode, leads to the ready identification of the zonal wavenumber  $k = F^{1/2} K$  of Figure 1. When the wavenumber is smaller than the cutoff wavenumber  $K_c = 2.399$ ,  $C_R$  is 0.5, implying that the unstable waves ( $C_I \neq 0, K < K_c$ ) in Eady's model propagate with the same speed (which is the basic current speed at the mid-level  $z = 0.5$ ), regardless of the wavelength. In view of the dispersive nature of the real atmospheric baroclinic unstable waves, it appears that some of the hitherto ignored mechanisms have to be included in the Eady model to bring it closer to realistic atmospheric situations.

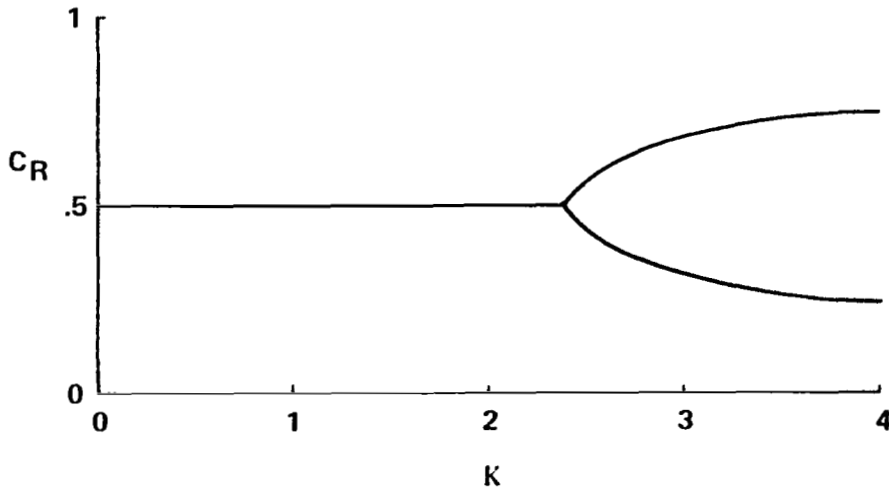


Figure 1. Propagation speed  $C_R$  versus scaled wavenumber  $K$ .

If  $K > K_C$ , equation (12) shows that  $C_I = 0$  and there are two branches of  $C_R$ , pointing to the existence of two neutral waves propagating with different speeds, one greater than and the other smaller than the wind speed at the mid-level. This point will be discussed further later.

The growth rate ( $K C_I$ ) is plotted in Figure 2. The unstable region ( $K < K_C = 2.40$ ) and the cutoff wavenumber  $K_C$  beyond which neutral waves exist are clearly shown. The most unstable wave, which is associated with the maximum growth rate, is seen to have wavenumber  $K \cong 1.6062$ . It is also apparent that in the unstable region ( $C_I \neq 0, K < K_C$ ), for every growing mode solution corresponding to  $C_I > 0$  there exists a damped wave with  $C_I < 0$ .

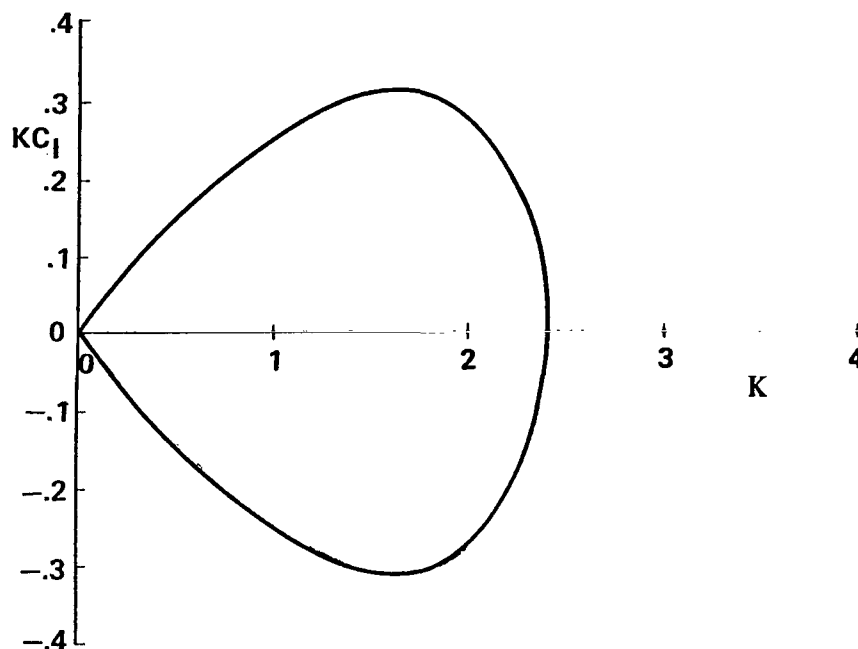
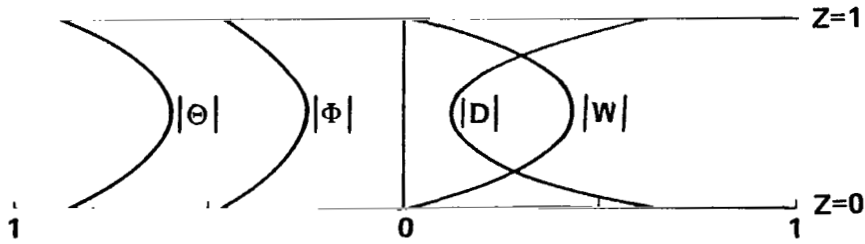


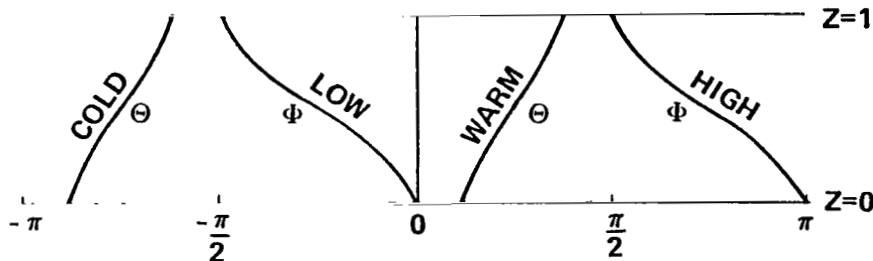
Figure 2. Growth Rate  $K C_I$  versus scaled wavenumber  $K$ .

We now present detailed information about the wave structure for the disturbances of varying zonal wavelengths. Since an eigenfunction is generally complex, the amplitude (or the modulus) and the phase will be displayed separately. For example, in the case of the perturbation pressure  $\Phi(z)$ ,

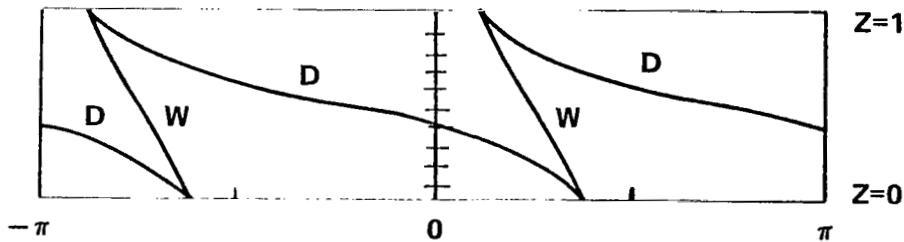
the amplitude,  $[A/(Q_2^2 + Q_3^2)] [(G_1^2 + G_2^2)^{1/2}]$ , and the negative value of the phase,  $-\tan^{-1}(G_2/G_1)$ , in accord with equations (15) and (16) are shown in Figures 3(a) and 3(b), respectively. Note that the eigenfunction solution of equation (8) contains an arbitrary constant  $A$ , which is set to be unity; therefore, the amplitude plots display only the relative magnitude of variation with  $z$ . Also, for the sake of better graphical presentation, different scale factors (for the plot of amplitude variations) and phase shift factors (for the plot of phase variations) are employed for each variable in the figures.



(a) Amplitude variations. Scale factors are 0.5 for  $|\Phi|$ , 0.5 for  $|\Theta|$ , 1.0 for  $|W|$ , and 0.3 for  $|D|$ .



(b) Negative relative phases of perturbation pressure  $\Phi$  and temperature  $\Theta$ . Phase shift factor is  $11.35^\circ$ .



(c) Negative relative phases of vertical velocity  $W$  and divergence  $D$ . Phase shift factor is  $11.35^\circ$ .

Figure 3. Amplitude and phase variations of the most unstable mode ( $K = 1.6061$ ,  $C_R = 0.5$ ,  $C_I = 0.1929$ ).

The wave structures of the most unstable mode are described in Figure 3. These plots may also be construed as being qualitatively representative of the wave structures of unstable waves in general. Because of the simple linear wind profile and the rigid boundary conditions, the amplitudes of the eigenfunctions of the Eady unstable waves are symmetrical with respect to the mid-level. The temperature and pressure perturbations are largest at the boundaries. The vertical velocity  $|W(z)|$  is zero at both boundaries and reaches the maximum at the mid-level. On the other hand, the horizontal divergence  $|D(z)|$  is a maximum at both boundaries and decreases to its minimum at the mid-level. Figures 3(b) and 3(c) show the vertical structure of the negative phase plot of the dynamical variables of the most unstable mode. The negative phase diagrams show the actual side view of the wave structures. Combining the amplitude and the negative phase information, the  $x$ - $z$  cross section over one wavelength is constructed in Figure 4 to illustrate the interrelations among dynamical variables. In Figure 4, the size of the letterings indicates the relative magnitude of the variables denoted. Both the pressure trough (high pressure, denoted by  $\Phi_+$ ) and the pressure ridge (low pressure, denoted by  $\Phi_-$ ) are tilted upward and backward. The warm tongue (the perturbation temperature maximum, denoted by  $\Theta_+$ ) lies ahead of the pressure trough but to the rear of the pressure ridge. Again, the cold tongue (the perturbation temperature minimum, denoted by  $\Theta_-$ ) is located at half-wavelength apart from the warm tongue. In a similar fashion, the vertical velocity distribution  $W$ , denoted by vertical arrows, and the horizontal divergence  $D$ , denoted by horizontal arrows, are marked in Figure 4. At the same time, the south-north ( $y$ ) component of velocity  $V$

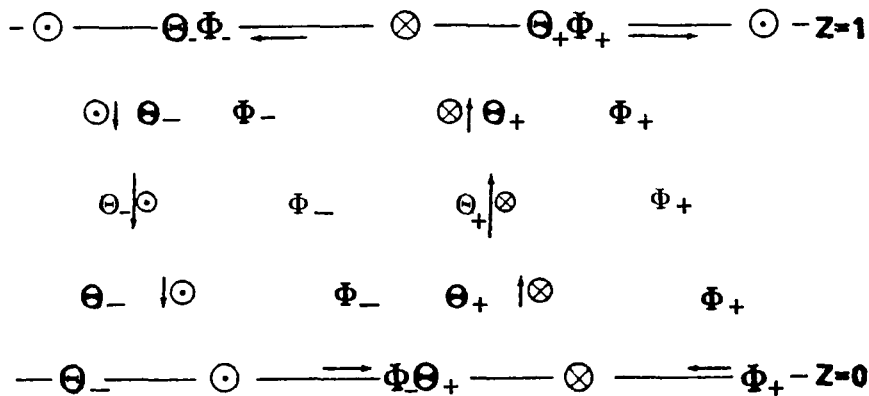
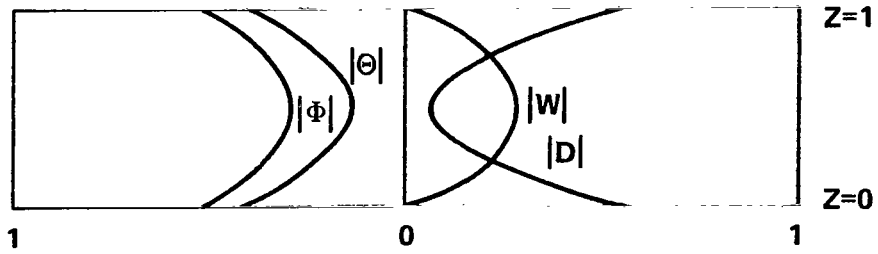


Figure 4. The  $x$ - $z$  plot showing the interrelationships among the dynamical variables. The size of the letterings indicates the relative magnitude of the variables.

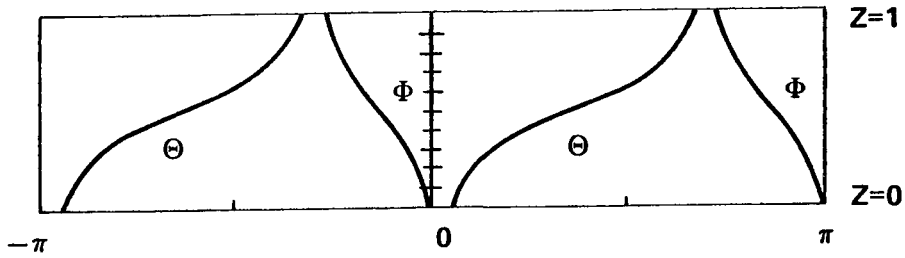
expressed in equation (17), which is shown by  $\otimes, \odot$  in Figure 4, has the same amplitude variation as the perturbation pressure  $\Phi$ , but the phase of  $V$  is  $\pi/2$  ahead of the phase  $\Phi$ . The  $x$ - $z$  cross section of Figure 4 reveals the well-known potential energy release mechanism associated with the baroclinically unstable waves [5]. If the kinetic energy of the wave field is to increase with time, the vertical velocity has to be positively correlated with the perturbation temperature so that on the average warm fluid rises while cold fluid falls. The correlation between  $w$  and  $\theta$  in Figure 4 for unstable waves verifies the preceding condition. Another significant aspect of the baroclinically unstable wave energetics is that the correlation between the south-north velocity component  $v$  and the perturbation temperature  $\theta$  should be positive, suggesting that the unstable waves, on the average, transport heat down the basic temperature gradient in the south-north direction. This is also shown in Figure 4; warm (cold) fluid is correlated with the velocity component into (out of) the plane of paper. In summary, the detailed wave structures of Figure 3, together with the  $x$ - $z$  plane plot, show how baroclinically unstable waves withdraw energy from the store of available potential energy of the basic current which is sustained by the latitudinally varying temperature field.

Now, it will be of interest to examine in detail the peculiar features of the baroclinic wave structures as the wavenumber  $K$  increases. Figure 5 illustrates the structure of an unstable mode at wavenumber  $K = 2.2$ , which has a reduced growth rate ( $C_R = 0.5$ ,  $C_I = 0.0961$ ). Although the overall patterns of the wave structure at this wavenumber are quite similar to those of the most unstable mode, some differences are easily discernible with respect to the negative phase diagrams of Figures 5(b) and 5(c). Whereas the phase line of  $\odot$  is further stretched toward the horizontal, the phase line of  $\Phi$  is more erect. Perhaps, the behavior of the vertical velocity  $W$  is the most interesting to analyze because other variables may be readily expressed in terms of  $W$  in the quasi-geostrophic formulation. The constant phase line of  $W$  of Figure 5(c) still slopes upward and backward, which is characteristic of unstable baroclinic waves; however, the slope is steeper (toward the vertical) than the case of the most unstable mode of Figure 3(c). This steepening of the phase line of  $W$  will become more apparent as the wavenumber approaches the cutoff wavenumber  $K_C$ .

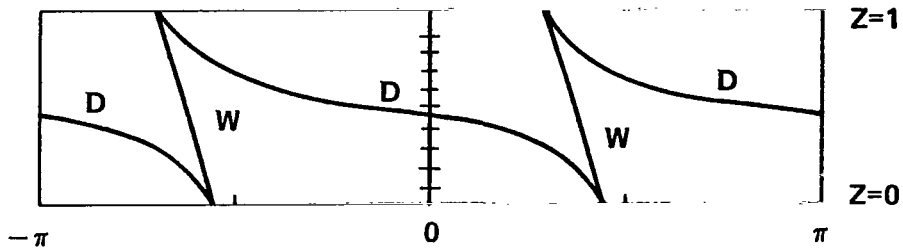
Figure 6 shows the structure of an unstable wave with the wavenumber closer to the cutoff wavenumber. At this wavenumber ( $K = 2.35$ ), the phase speed is still 0.5, but the growth rate is quite small ( $C_I = 0.0476$ ). The phase lines of  $\odot$  and  $D$  are further stretched toward the horizontal, and a trend may be recognized in that the phase lines of  $\odot$  and  $D$  tend to a step-like shape. However, the phase lines of  $\Phi$  and  $W$  are further steepened toward the vertical.



(a) Amplitude variations. Scale factors are 0.5 for  $|\Phi|$ , 0.2 for  $|\Theta|$ , 0.25 for  $|W|$ , and 0.1 for  $|D|$ .

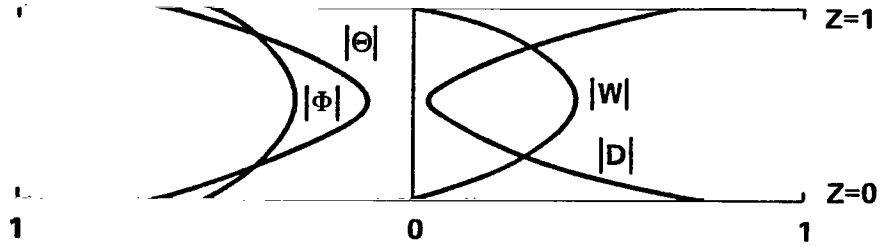


(b) Negative relative phases of perturbation pressure  $\Phi$  and temperature  $\Theta$ . Phase shift factor is  $5.13^\circ$ .

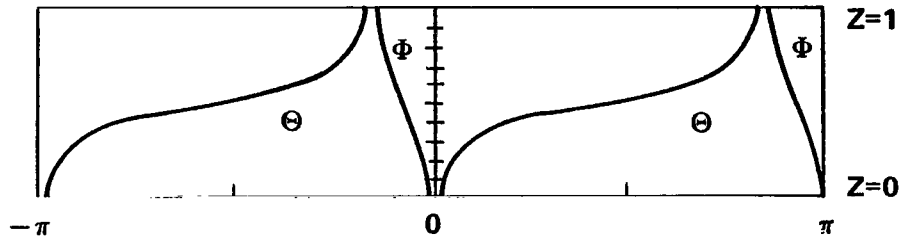


(c) Negative relative phases of vertical velocity  $W$  and divergence  $D$ . Phase shift factor is  $5.13^\circ$ .

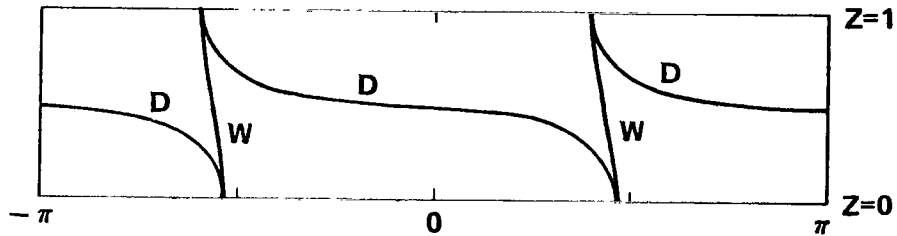
Figure 5. Amplitude and phase variations of an unstable wave ( $K = 2.2$ ,  $C_R = 0.5$ ,  $C_I = 0.0961$ ). The wavenumber  $K (= 2.2)$  is greater than the wavenumber of the most unstable mode  $K = 1.6061$ .



(a) Amplitude variations. Scale factors are 0.5 for  $|\Phi|$ , 0.3 for  $|\Theta|$ , 0.3 for  $|W|$ , and 0.1 for  $|D|$ .



(b) Negative relative phases of perturbation pressure  $\Phi$  and temperature  $\Theta$ . Phase shift factor is  $2.49^\circ$ .



(c) Negative relative phases of vertical velocity  $W$  and divergence  $D$ . Phase shift factor is  $2.49^\circ$ .

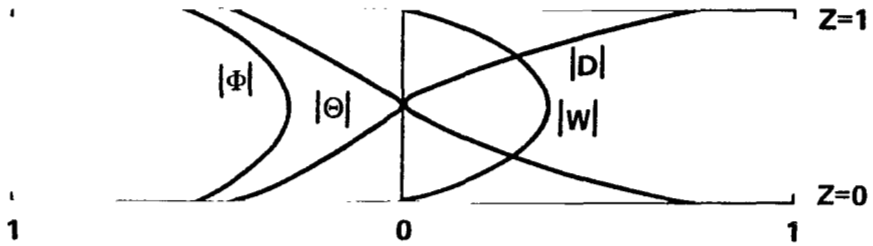
Figure 6. Amplitude and phase variations of an unstable wave ( $K = 2.35$ ,  $C_R = 0.5$ ,  $C_I = 0.0476$ ). The wavenumber  $K (= 2.35)$  is close to the critical wavenumber  $K_C$ .

When the wavenumber equals the critical wavenumber, we have a marginally stable mode. The structure of this marginally stable mode ( $K = 2.3993$ ,  $C_R = 0.5$ ,  $C_I \cong 0$ ), as shown in Figure 7, exhibits features which are the limiting behavior of the unstable waves. For this marginally stable mode, the amplitude functions of Figure 7(a) are still symmetric with respect to the mid-level. Both the temperature perturbation  $\Theta$  and the horizontal divergence  $D$  vanish at the mid-level. The phase lines of  $\Phi$  and  $W$  are now vertical, and the phase lines of  $\Theta$  and  $D$  are step functions with steps at the mid-level. These vertical phase line patterns are typical of the neutral waves ( $C_I = 0$ ) in general, where the mechanism for converting energy from the basic current to perturbations is absent. Tokioka [6], by computing the energy transfer rate in terms of the vertical velocity, demonstrated that the phase line of  $W$  is vertical [i.e.,  $d\alpha/dz = 0$ , if  $W$  is written as  $W = |W| \exp(i\alpha)$ ] when there is no energy release from the basic state to the disturbances.

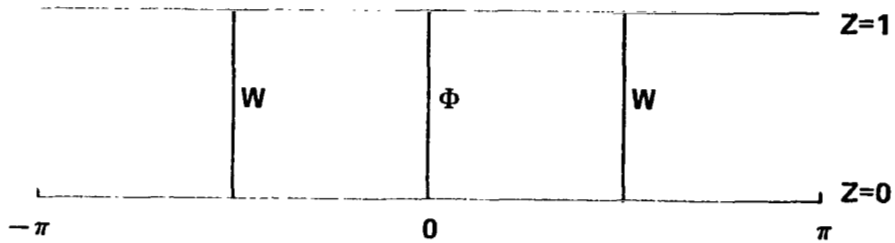
In the stable wave region where the wavenumber is larger than the cutoff wavenumber, as is shown in the eigenvalue plots of Figures 1 and 2, there appear two neutral modes ( $C_I = 0$ ), each of which has a different phase speed  $C_R$ , one larger than and the other smaller than the basic current speed at the mid-level.

The wave structure of a fast-propagating ( $C_R > 0.5$ ) neutral mode ( $K = 3.5$ ,  $C_R = 0.7131$ ,  $C_I = 0$ ) is shown in Figure 8. For this neutral mode, the amplitude functions of Figure 8(a) are no longer symmetric with respect to the mid-level. It is also evident that the amplitude distribution functions are enhanced in the region near the upper boundary. The perturbation temperature  $\Theta$  is zero at a level in the lower half of the fluid depth, and the phase line of  $\Theta$  has a step at this level. The horizontal divergence  $D$  becomes zero at a level between the mid-level and the upper boundary, and the phase line of  $D$  has a step at this level. As was pointed out earlier, the phase lines of  $\Phi$  and  $W$  are vertical, allowing no energy conversion mechanism from the basic state to the disturbance.

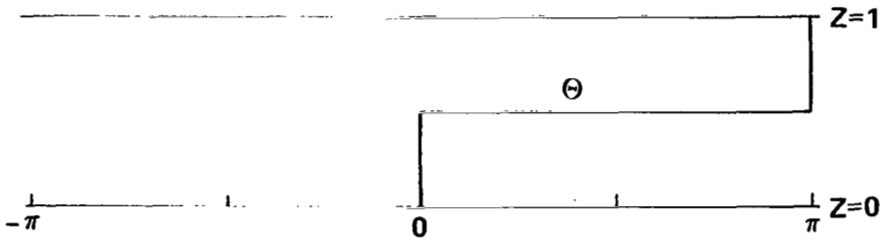
The wave structure of a slow-propagating ( $C_R < 0.5$ ) neutral mode ( $K = 3.5$ ,  $C_R = 0.2869$ ,  $C_I = 0$ ) is shown in Figure 9. The bulk of the disturbance is confined to the bottom half-depth of the fluid. This slow-propagating neutral mode exhibits features opposite to the fast-propagating neutral mode described in Figure 8.



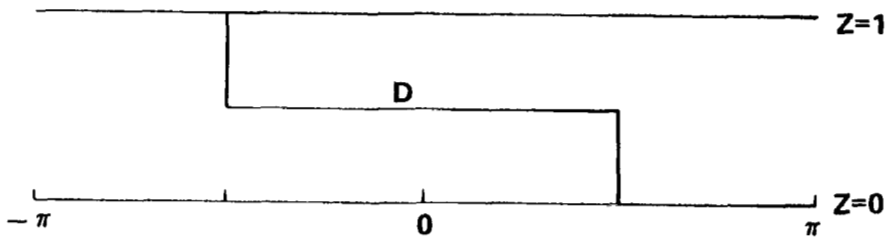
(a) Amplitude variations. Scale factors are 0.5 for  $|\Phi|$ , 0.2 for  $|\Theta|$ , 0.25 for  $|W|$ , and 0.1 for  $|D|$ .



(b) Negative relative phases of vertical velocity  $W$  and perturbation pressure  $\Phi$ . Phase shift factor is 0.0.

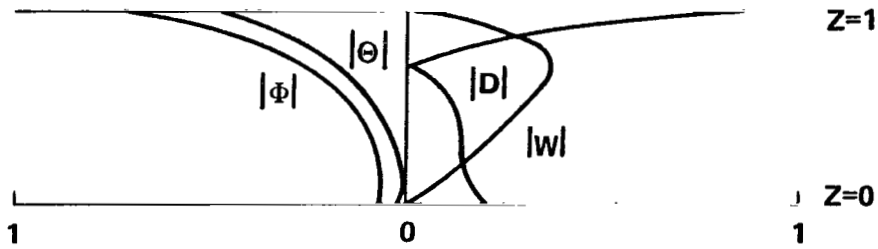


(c) Negative relative phase of perturbation temperature  $\Theta$ . Phase shift factor is 0.0.

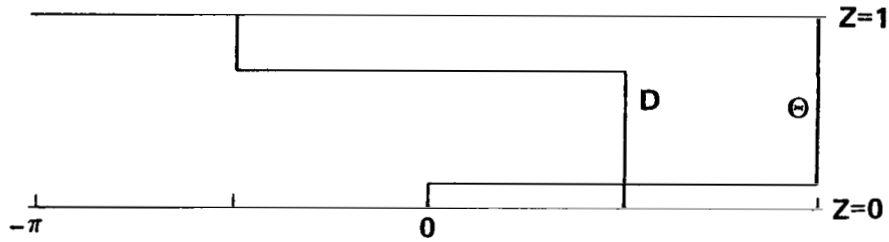


(d) Negative relative phase of divergence  $D$ . Phase shift factor is 0.0.

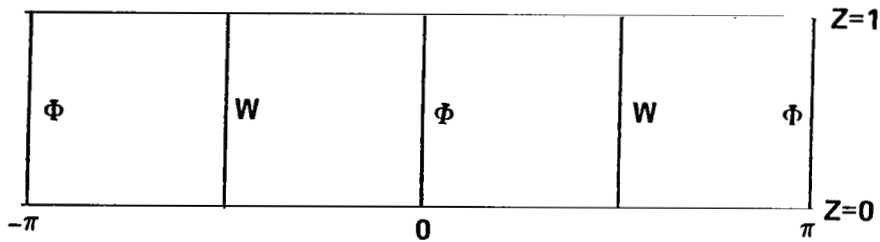
Figure 7. Amplitude and phase variations of a marginally stable mode ( $K = 2.3996$ ,  $C_R = 0.5$ ,  $C_I = 0.0$ ).



(a) Amplitude variations. Scale factors are 0.5 for  $|\Phi|$ , 0.1 for  $|\Theta|$ , 0.2 for  $|W|$ , and 0.05 for  $|D|$ .

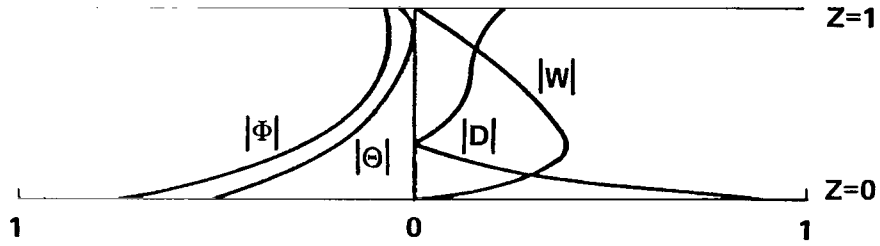


(b) Negative relative phases of perturbation temperature  $\Theta$  and divergence  $D$ . Phase shift factor is 0.0.

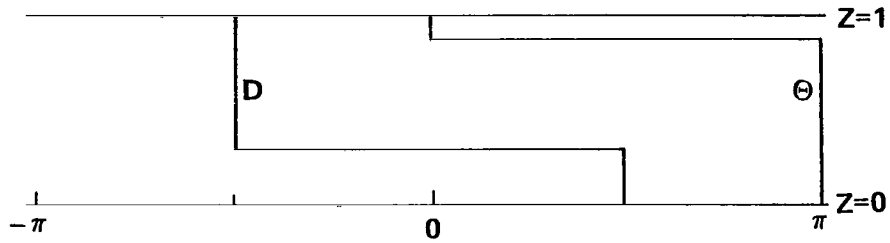


(c) Negative relative phases of vertical velocity  $W$  and perturbation pressure  $\Phi$ . Phase shift factor is 0.0.

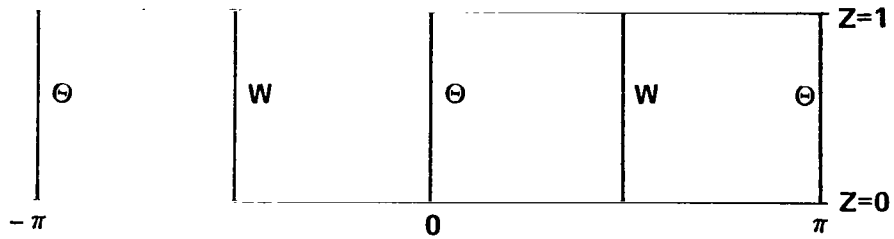
Figure 8. Amplitude and phase variations of a fast-propagating stable mode ( $K = 3.5$ ,  $C_R = 0.7131$ ,  $C_I = 0.0$ ).



(a) Amplitude variations. Scale factors are 0.5 for  $|\Phi|$ , 0.1 for  $|\Theta|$ , 0.2 for  $|W|$ , and 0.05 for  $|D|$ .



(b) Negative relative phases of perturbation temperature  $\Theta$  and divergence  $D$ . Phase shift factor is 0.0.



(c) Negative relative phases of vertical velocity  $W$  and perturbation pressure  $\Phi$ . Phase shift factor is 0.0.

Figure 9. Amplitude and phase variations of a slow-propagating stable mode ( $K = 3.5$ ,  $C_R = 0.2869$ ,  $C_I = 0.0$ ).

A physical interpretation is helpful in explaining the transition from the neutral modes to the unstable modes as the wavelength increases. In the stable region ( $K > K_C$ ) the horizontal length scale (i.e., wavelength)  $L_s$  is small so that the corresponding penetration scale height [7,8], of the order of  $fL_s/N$ , is smaller than the half-depth of the fluid. As a consequence, the motion forced by the external conditions at the rigid boundaries cannot penetrate fully into the interior of the fluid. The resulting motion is thus concentrated in regions adjacent to the boundaries. Under these circumstances, the two neutral modes, energetically incapable of converting potential energy from the basic current to the disturbances, are simply advected by the basic current. Since the basic current is linearly increasing with  $z$ , the mode whose motion is concentrated near the upper boundary is advected faster than the mode whose motion is concentrated near the bottom boundary.

As the wavelength increases to the point where the penetration scale height becomes comparable to the half-depth of the fluid, the two neutral modes coalesce to form a single mode, and instability begins to set in.

## REFERENCES

1. Charney, J. G.: The Dynamics of Long Waves in a Baroclinic Westerly Current. *J. of Meteor.*, vol. 4, 1947, p. 135.
2. Eady, E. T.: Long Waves and Cyclone Waves. *Tellus*, vol. 1, 1949, p. 33.
3. Pedlosky, J.: The Stability of Currents in the Atmosphere and the Ocean: Part I. *J. Atmos. Sci.*, vol. 21, 1964, p. 201.
4. Phillips, N. A.: An Overlooked Aspect of the Baroclinic Stability Problem. *Tellus*, vol. 16, 1964, p. 268.
5. Pedlosky, J.: Geophysical Fluid Dynamics. *Mathematical Problems in the Geophysical Sciences*, edited by W. H. Reid. American Mathematical Society, Providence, Rhode Island, 1971, p. 1.
6. Tokioka, T.: Non-geostrophic and Non-hydrostatic Stability of a Baroclinic Fluid. *J. of Meteor. Soc. Japan*, vol. 48, 1970, p. 503.
7. McIntyre, M. E.: On the Non-separable Baroclinic Parallel Flow Instability Problem. *J. Fluid Mech.*, vol. 40, 1970, p. 273.
8. Walin, G.: Some Aspects of Time-dependent Motion of a Rotating Stratified Fluid. *J. Fluid Mech.*, vol. 36, 1969, p. 289.

1. REPORT NO. NASA TP-1548		2. GOVERNMENT ACCESSION NO.		3. RECIPIENT'S CATALOG NO.	
4. TITLE AND SUBTITLE  The Wave Structures of the Eady Model of Baroclinic Instability				5. REPORT DATE October 1979	
7. AUTHOR(S) Jae Min Hyun* and William W. Fowlis				6. PERFORMING ORGANIZATION CODE	
9. PERFORMING ORGANIZATION NAME AND ADDRESS  George C. Marshall Space Flight Center Marshall Space Flight Center, Alabama 35812				8. PERFORMING ORGANIZATION REPORT #	
12. SPONSORING AGENCY NAME AND ADDRESS  National Aeronautics and Space Administration Washington, D. C. 20546				10. WORK UNIT, NO. M-289	
15. SUPPLEMENTARY NOTES  Prepared by Space Sciences Laboratory, Science and Engineering *NAS/NRC Senior Postdoctoral Research Associate				11. CONTRACT OR GRANT NO.	
16. ABSTRACT  A comprehensive analysis is presented of the wave structures of the Eady model of baroclinic instability. By solving the linear quasi-geostrophic set of equations pertinent to the Eady model, the complex eigenvalues and the eigenfunctions are obtained. The propagation speed and the growth rate are computed. Detailed quantitative information is provided about the wave structures for several unstable modes, a marginally stable mode, and a stable mode. The peculiarities concerning the amplitude and the phase variations of the waves are noted as the wavenumber varies from the unstable region to the stable region. Physical interpretations of the interrelationships among the dynamical variables are given, with a view toward revealing important aspects of the energy transfer from the basic state to the growing waves.				13. TYPE OF REPORT & PERIOD COVERED  Technical Paper	
17. KEY WORDS  Baroclinic instability Eady model Quasi-geostrophic set Wave structures				14. SPONSORING AGENCY CODE	
18. DISTRIBUTION STATEMENT  Category 47					
19. SECURITY CLASSIF. (of this report)  Unclassified		20. SECURITY CLASSIF. (of this page)  Unclassified		21. NO. OF PAGES  26	22. PRICE  \$4.00

\*For sale by the National Technical Information Service, Springfield, Virginia 22161

National Aeronautics and  
Space Administration

Washington, D.C.  
20546

Official Business

Penalty for Private Use, \$300

THIRD-CLASS BULK RATE

Postage and Fees Paid  
National Aeronautics and  
Space Administration  
NASA-451



8 1 1U,E, 092479 S00903DS  
DEPT OF THE AIR FORCE  
AF WEAPONS LABORATORY  
ATTN: TECHNICAL LIBRARY (SUL)  
KIRTLAND AFB NM 87117

**NASA**

S

ER: If Undeliverable (Section 158  
Postal Manual) Do Not Return